



Preparation of superparamagnetic iron oxide nanoparticles and evaluation of their adsorption capacity toward carbamazepine and diatrizoate

Soon Uk Yoon, Biswanath Mahanty, Chang Gyun Kim*

Department of Environmental Engineering, INHA University, Incheon, Korea, Tel. +82 32 876 2351;

email: suyoon@inha.edu (S.U. Yoon), Tel. +82 32 860 8988; email: bmahanty@inha.ac.kr (B. Mahanty), Tel. +82 32 860 7561;

email: cgk@inha.ac.kr (C.G. Kim)

Received 30 December 2014; Accepted 19 June 2015

ABSTRACT

Carbamazepine (CBZ) and diatrizoate (DTZ) are from the group of pharmaceutical and personal care products known to be persistent and non-biodegradable in wastewater treatment. Adsorptive removal of CBZ and DTZ using superparamagnetic iron oxide (magnetite, Fe_3O_4) nanoparticles (NPs), along with those coated with either methacrylic acid (MAA), $\text{Al}(\text{OH})_3$, or SiO_2 were evaluated. Transmission electron microscopy and scanning electron microscopy analyzes revealed that the NPs were about 10 nm in diameter. Fourier transform infrared analysis confirmed the presence of carboxyl group on MAA-coated NPs, and hydroxyl group on alumina- and silica-coated NPs. Results suggest that the major fraction of the drugs is adsorbed by the NPs in about 6–8 h. Maximum DTZ adsorption capacities (based on Freundlich isotherm) of MAA-, $\text{Al}(\text{OH})_3$ -, and SiO_2 -coated NPs (112.46, 82.20, and 90.48 mg/g, respectively) were much higher than that of the uncoated NPs (66.17 mg/g). Based on batch adsorption studies, an optimal adsorption condition was proposed, i.e. CBZ and DTZ concentration of 100 $\mu\text{g}/\text{L}$, 0.05 g of NPs, adjusted pH of 8, and exposure time of 7 h. At this condition, the maximum adsorption of CBZ was about 32.7, 47.3, 51.1, and 50.2% with uncoated, MAA-coated, $\text{Al}(\text{OH})_3$ -coated, and SiO_2 -coated NPs, respectively. The equivalent removal for DTZ by the NPs was at 44.3, 52.8, 60.6, and 38.1%, respectively. Further desorption studies revealed that about 85.56 and 78.00% of adsorbed CBZ and DTZ can be readily released from $\text{Al}(\text{OH})_3$ - and MAA-coated NPs, respectively.

Keywords: Carbamazepine; Diatrizoate; Iron oxide nanoparticles

1. Introduction

The long-resistance pharmaceuticals released along with house sewer, hospital waste, and industrial wastewater are known to have significant impact on

the receiving environment [1]. These materials are generally non-degradable and remain stable during passage through wastewater treatment plants, resulting in potential toxicity to human health and the ecosystem [2]. Carbamazepine (CBZ) has an array of pharmaceutical applications, most importantly as an anticonvulsant, and when metabolized yields a

*Corresponding author.

Presented at the 7th International Conference on Challenges in Environmental Science and Engineering (CESE 2014) 12–16 October 2014, Johor Bahru, Malaysia

number of metabolites. Although the environmental concentration of CBZ is very nominal (surface water 647 ng/L and groundwater 610 ng/L), even these small fractions tend to evade treatment and are finally discharged into surface waters. This route of exposure probably explains the emergence of CBZ as the most commonly found pharmaceutical and personal care product in the environment [3]. On other hand, chemically inert diatrizoate (DTZ) is widely used as iodinated X-ray contrast media and often administrated at very high doses [4,5].

Research has recently focused on synthetic methods for preparing iron oxide nanoparticles (NPs) with high specific surface area [6,7]. Apart from the associated useful physical properties, their magnetic property can be of additional advantage in contaminant capture during water purification process, where NP-adsorbed contaminants can be separated from treated water with magnetic force [8,9]. However, pure magnetic particles themselves may not be very useful as they tend to form large aggregates due to their anisotropic dipolar attraction, or become structurally changed, which alters their magnetic properties [10]. Therefore, a suitable coating is essential to overcome such limitations. Surface modification techniques are also being developed to fine-tune the absorption process [11,12].

Passive surface coating of the iron oxide NPs with inorganic or organic materials (e.g. silica, methyl methacrylate) not only offers improved stability, but also the different surface groups (such as silanol and carboxyl) can interact with specific ligands [13]. Methacrylic acid (MAA), as a precursor for methyl methacrylate and poly-MAA, is used in the production of various polymers and copolymers. The carboxyl group in MAA can improve the dispersion of coated particles in biological systems by shifting the isoelectric point [14]. On other hand, inorganic hydrous aluminum oxide $\text{Al}(\text{OH})_3$, well known for its high affinity adsorption in defluoridation studies, can be a useful surface modifier for iron oxide NPs [15]. SiO_2 composite microspheres have also been shown to be an effective adsorbent offering a recyclable approach for removing inorganic pollutants from water [16].

In this study, we selected three different surface coatings, viz., MAA, $\text{Al}(\text{OH})_3$, and SiO_2 , on iron oxide NPs for their possible use in the removal of CBZ and DTZ from water. Adsorption kinetic, isotherm, and subsequent desorption behavior were studied using the three surface-coated and uncoated NPs in batch experiments. The variability in their adsorption capacities are discussed in terms of surface charge and influence of influent pH.

2. Materials and methods

2.1. Chemicals and materials

Reagent grade iron(II) chloride tetrahydrate ($\text{FeCl}_2 \cdot 4\text{H}_2\text{O}$) and iron(III) chloride hexahydrate ($\text{FeCl}_3 \cdot 6\text{H}_2\text{O}$) were purchased from Sigma-Aldrich (USA). Sodium hydroxide pellets of 98% purity were purchased from Duksan (Korea). MAA, aluminum hydroxide, potassium peroxydisulfate ($\text{K}_2\text{S}_2\text{O}_8$), sodium dodecyl sulfate (SDS), sodium metasilicate for surface functionalization of iron oxide NPs, and target materials (CBZ and DTZ) were purchased from Sigma-Aldrich (USA).

2.2. Synthesis of iron oxide NPs

The super paramagnetic iron oxide NPs were synthesized by the co-precipitation of ferrous and ferric ions in sodium hydroxide solution [17]. Briefly, an aqueous solution of Fe ions with a molar ratio of Fe (II)/Fe(III) = 1:2 was prepared by dissolving $\text{FeCl}_2 \cdot 4\text{H}_2\text{O}$ and $\text{FeCl}_3 \cdot 6\text{H}_2\text{O}$ in 50 mL of deionized water. The resulting solution was added in a dropwise manner into 100 mL of 1 M NaOH solution maintained at about 70°C under mechanical stirring. Upon introduction of the Fe ions, the NaOH solution turned black. Thereafter, the reaction mixture was stirred for a further 30 min and the precipitate was recovered using an external magnetic bar. The precipitate was washed three times with deionized water and then subjected to ultrasonic treatment before functionalization.

2.3. Functionalization of the iron oxide NPs using organic–inorganic materials

2.3.1. Functionalizing by MMA

The iron oxide NPs were coated with MAA based on the approach proposed by Yu and Chow [14]. Briefly, 0.3 g of dried iron oxide NPs was dispersed in distilled water by ultrasonic treatment. The NPs suspension was mixed with 200 mL of SDS solution (5.75 g/L), heated to 70°C, and then 0.96 mL of MAA was introduced into the flask and the pH was adjusted to three using H_2SO_4 . The reaction mixture was equilibrated for about 45 min at the same temperature before 1.98 g of $\text{K}_2\text{S}_2\text{O}_8$ initiator was added. The polymerization reaction was carried out at 70°C in an argon atmosphere for 2 h, followed by cooling to room temperature. The isolated magnetic NPs were redispersed in deionized water under ultrasonication, followed by recovery using an external magnetic field. The washing process was repeated at least three times. A portion of the washed magnetic particles was

subsequently dried for physical characterization. The remaining NPs were dispersed in 250 mL of deionized water and kept for drug adsorption experiments.

2.3.2. Functionalizing by $Al(OH)_3$

The synthesized iron oxide NPs were coated with $Al(OH)_3$ as proposed by Zhao et al. [15]. Aluminum nitrate solution (1 M) was added in a dropwise manner into the iron oxide NP suspension (mass ratio of Fe_3O_4 to $Al(OH)_3$ at 2:5) and within 1 h the pH of the mixture was adjusted to 8.0 by the addition of 2 M NaOH. The mixture was further stirred for 2 h, while maintaining a constant temperature of 80°C. Finally, the coated NPs were thoroughly washed and resuspended in deionized water.

2.3.3. Functionalizing by SiO_2

SiO_2 -coated iron oxide NPs were prepared based on the method described by Hu et al. [16]. Briefly, 200 mL of Fe_3O_4 suspension was added to 100 mL of aqueous sodium metasilicate (Na_2SiO_3) solution (13 g/L) and the pH was adjusted to 6.0 with 1 M HCl. The mixture was mechanically stirred for 3 h maintaining a constant temperature of about 80°C. Finally, the SiO_2 -functionalized iron oxide NPs were recovered with an external magnet washed twice with deionized water and dried under vacuum at 60°C.

2.4. Characterization of the functionalized NPs

Surface chemical properties of synthesized NPs were investigated with a transmission electron microscopy (TEM; JEM2100F, JEOL, Japan), scanning electron microscopy (SEM; S-4300SE, Hitachi, Japan), and Fourier transform infrared (FT-IR; VERTEX 80V, Bruker, Germany) spectroscopy.

For TEM analysis, 10 mg of dry NPs preparation was dispersed in water by ultrasound for about 6 h in a conical tube and then about three drops were applied over the TEM grid (Ted Pella®, USA). The sample grid was dried for 24 h in a vacuum desiccator before analysis. For SEM, about 1 mg of the air-dried NP preparation was placed on an aluminum plate and attached with a double-sided tape for zirconium coating using a precision etching and coating system (Gatan 682 PECS™, Hitachi, Japan). For FT-IR, dried powder samples were mixed into KBr in a weight ratio of 1:4 and compressed to 1-mm thick, spectroscopic grade KBr pellets.

2.5. Adsorption kinetic and isotherm studies

The three different types of surface-coated and uncoated original iron oxide NPs were evaluated for their adsorption capacity toward the tested drugs (CBZ and DTZ) by varying the drug concentration, absorbent amount, suspension pH, and equilibrium time. The experimental variables adopted in adsorption kinetics, adsorption isotherm, and equilibrium adsorption under varying pH incubation conditions is summarized in Table 1. Irrespective of the nature of investigation, each of the four NP types were well dispersed by ultrasound, and added into influent solution containing CBZ or DTZ and incubated under stirring condition (250 rpm) at 30°C.

2.6. Desorption of CBZ and DTZ from coated and uncoated NPs

Desorption of CBZ and DTZ was performed by adding the drug-adsorbed NPs (50 mg) recovered from adsorption study to 100 ml of fresh aqueous solution at a pH that offered least adsorption in earlier screening experiments (see Section 2.5). During the desorption

Table 1
Experimental variables adopted in different adsorption studies

Experiment	Volume (ml)	Drug conc. ($\mu\text{g/L}$)	Nanoparticle (NP) amount (g)	pH	Incubation time (h)
Adsorption kinetics	500	100	0.05	8	Variable ^a
Adsorption isotherm	100	100	Variable ^b	8	3
Effect of incubation pH	100	100	0.05	Variable ^c	3
Adsorption isotherm model	100	Variable	0.05	8	3
Optimized adsorption ^d	500	100	0.05	8	7

^aSampling points were distributed every 2 h up to 18 h and final sample were taken on 24th hour.

^bNP amount was 0.01, 0.02, 0.03, 0.05, and 0.10 g in different subsets.

^cInitial pH of adsorption experiments was adjusted to 5–9.

^dIn optimized adsorption experiment with Fe_3O_4 NPs the pH was adjusted to 6.

study, liquid phase samples (20 ml each) were taken every two hours and replaced with an equivalent volume of fresh desorbing solution. The concentration of CBZ or DTZ in the samples was measured after solid phase extraction (SPE) and high performance liquid chromatography (HPLC). The quantitative loss in sampling and dilution from fresh solvent replacement was appropriately corrected while calculating the percentage of drug desorbed from the NPs.

2.7. Solid phase extraction (SPE) and HPLC of CBZ and DTZ

The aqueous phase concentration of CBZ and DTZ in adsorption or desorption tests was analyzed through SPE and HPLC (Agilent technology 1200 series) [17]. Preprocessed filtrates were extracted in HLB (Oasis™) and ENV+ (Waters®) SPE cartridges. The cartridges were installed on a vacuum manifold and conditioned with methanol and deionized water. Thereafter, the samples were preadjusted to pH 2.7 by 3.5 M H₂SO₄ and then allowed to pass through the cartridges at a rate of 15 mL/min. The cartridges were washed twice with 3 mL double distilled water and then dried under vacuum for 10 min. Finally, CBZ and DTZ were eluted with 3 × 3 mL of methanol dripping under vacuum. The eluted CBZ and DTZ fractions were pooled and concentrated (about 1 mL) in a nitrogen gas-aided evaporation system (TurboVap®).

HPLC analysis of the concentrated samples was carried out in a Zorbax Eclipse XDB-C18 column (4.8 × 150 mm, 5 μm, Agilent technology). A binary gradient consisting of 0.1% v/v formic acid solution and methanol at a flow rate of 1 mL/min was adopted while UV detection at 258 nm was utilized. The mobile phase gradient was maintained as follows: 5% methanol held for 3.5 min, increased linearly to 50% by 5 min and held for 2 min, increased linearly to 60 and 80% every 2 min and held for 2 min, respectively, and finally stepped to 100% for 16 min. The column was washed with 100% methanol to remove any residue in-between sample runs.

3. Result and discussion

3.1. Characterization of NPs

The original iron oxide NPs synthesized by co-precipitation had a size less than 10 nm as evident in TEM analysis (Fig. 1(a)). For coated NPs, a core-shell structure arrangement was discernible. For MAA-coated NPs, one or more iron oxide NPs core appeared to have been embedded inside the organic polymer shell coat. However, structural irregularity in

the Al(OH)₃-coated particles, possibly from overlapping particles, made such assessment more difficult. In the silica-coated NPs, a darker core and lighter shell can be distinguished.

The results of surface component analysis in SEM and EDAX for the three differently coated NPs are shown in Figs. 2 and 3, respectively.

The SEM images of the NPs clearly revealed the floc and porosity on the surface texture, which provides the adsorbents with large surface areas and high adsorption capacity. On other hand, Al(OH)₃-coated Fe₃O₄ NPs appeared to be monodispersed. Elemental information about the surface composition of resulting NPs was confirmed by EDAX. The EDAX results also showed that the MAA-coated iron oxide NP surface had much higher carbon content (63.78%) than that of the uncoated one (48.68%). As expected, Al(OH)₃- and SiO₂-coated NP surfaces contained 41.98% Al and 11.61% Si components, respectively.

FT-IR reveals the functional groups on the particle surface. FT-IR results in Fig. 4 show strong absorption bands at 631 and 570 cm⁻¹ confirming that the main phase of iron oxide samples was magnetite [18]. The broad band at 3,400–3,500 cm⁻¹ indicated the presence of surface hydroxyl groups in iron oxide NPs with MAA coating. The observed C–H stretching bands (2,917 and 2,856 cm⁻¹) suggested the presence of MAA on the surface of the magnetite NPs. The lower intensity O–H band (3,400–3,500 cm⁻¹) in MAA-coated NPs in comparison to the uncoated magnetite was attributed to abstraction of surface hydroxyl groups from the magnetite NPs with reaction of the carboxylic acid group in MAA [14]. Aluminum hydroxide NP peaks at 1,076 and 1,350 cm⁻¹ suggested Al–O–Al bond and Al–O–H bond, respectively [19]. Impregnation of SiO₂ molecules on Fe₃O₄ surface was confirmed from the strong Si–O band around 1,093 cm⁻¹. A weaker and broadband around 3,400 cm⁻¹ suggested hydrogen-bonded O–H stretching [16].

3.2. Evaluation of adsorptive capacity toward CBZ and DTZ

3.2.1. Adsorption kinetics

The adsorption kinetics of CBZ and DTZ by the different NPs are shown in Fig. 5. The adsorption rates were moderately fast for both coated and uncoated NPs, where the maximum amount of drugs was actually adsorbed within the initial couple of hours. At equilibrium, uncoated NPs showed about 40.99 and 47.63% removal for CBZ and DTZ, respectively. Removal of CBZ by the MAA-, Al(OH)₃- and SiO₂-coated NPs was 56.28, 47.83, and 50.94%,

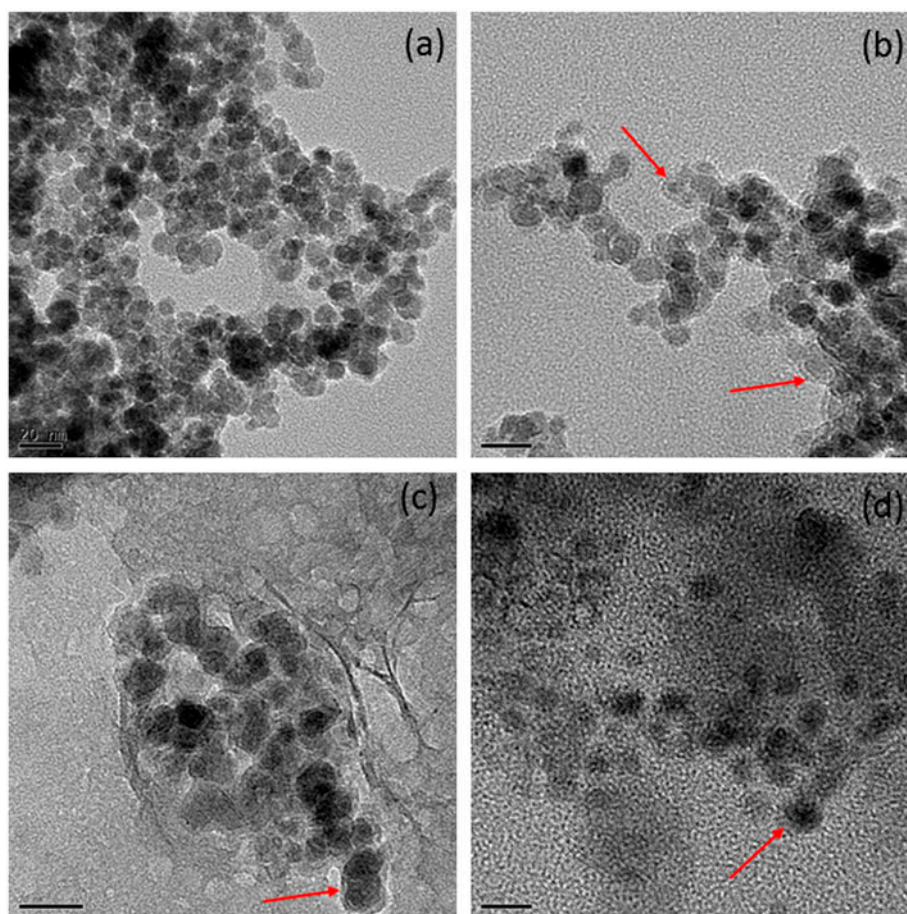


Fig. 1. TEM images of (a) uncoated, (b) MAA-coated, (c) $\text{Al}(\text{OH})_3$ -coated, and (d) SiO_2 -coated iron oxide nanoparticles (NPs). The discernible core-shell structure of the coated NPs is indicated with a red arrow. Shown scale bar is 20 nm.

compared to 57.72, 50.28, and 53.04% for DTZ removal, respectively.

3.2.2. Adsorption isotherm

Varying the adsorbent dosage relative to the fixed initial spike of CBZ and DTZ was used to analyze the adsorption isotherm. Each of the four adsorbents was tested at 10, 20, 30, 50, and 100 mg, while keeping CBZ and DTZ at 100 $\mu\text{g}/\text{L}$. The equilibrium aqueous phase concentrations in the different batch experiments are shown in Fig. 6. The equilibrium adsorption capacity (as well as the total amount of CBZ and DTZ adsorbed) continued to increase with increasing adsorbent dosages. However, once a critical adsorbent dosage (viz. 0.05 g) is attained, no further enhancement in adsorption capacity is noted. As expected, for a fixed initial solute (CBZ or DTZ) concentration, increasing adsorbent dose provided more adsorption

sites, which decreased the equilibrium concentration and the adsorption capacity.

3.2.3. Effect of pH on adsorption efficiency

The equilibrium adsorption capacity of different NPs under varying influent pH is shown in Fig. 7. CBZ adsorption by uncoated iron oxide NPs decreased with increasing influent pH above 6. Although CBZ adsorption by the three differently coated iron oxide NPs was lower than that of the uncoated one at lower pH range, this trend was reversed at pH over 7. At influent pH 8, the SiO_2 - and $\text{Al}(\text{OH})_3$ -coated NP adsorbed 0.073 and 0.069 $\mu\text{g}/\text{mg}$ of CBZ, respectively—much higher than the respective amounts adsorbed at pH 6 (0.023, 0.017 $\mu\text{g}/\text{mg}$).

CBZ ($\text{p}K_a$ is 14.0) does not dissociate in acidic solutions [20]. At low pH ($< \text{pH}_{\text{zpc}} \cong 8$), iron oxides are positively charged, which results in a very weak

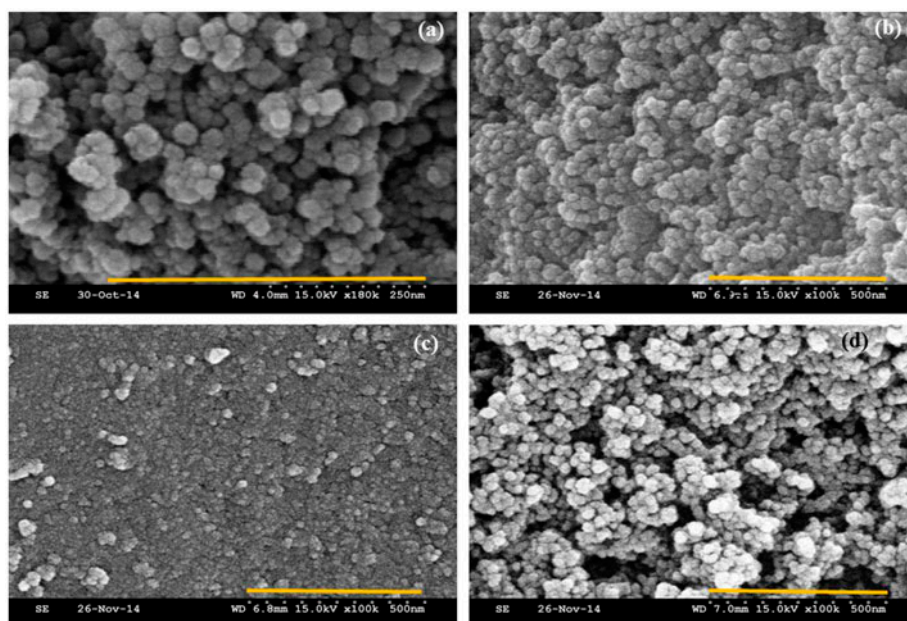


Fig. 2. SEM images of (a) uncoated, (b) MAA-coated, (c) Al(OH)₃-coated, and (d) SiO₂-coated iron oxide nanoparticles (NPs). Scale bar 500 nm.

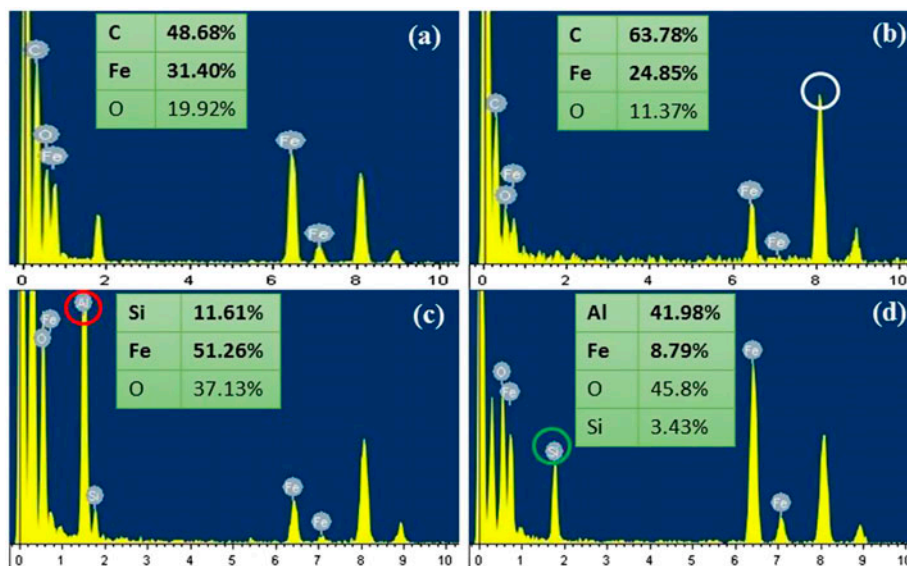


Fig. 3. EDX spectra of (a) uncoated, (b) MAA-coated, (c) Al(OH)₃-coated, and (d) SiO₂-coated iron oxide nanoparticle (NPs) with their surface elemental composition (wt.%). Relevant elemental peaks for C, Al, and Si in the coated NPs are highlighted with white, red, and green circles, respectively. The horizontal axis of spectrum is in keV.

binding with unionized CBZ [21]. On other hand, the carboxyl group in MAA activates at pH over 3.5, which can offer better adsorption capacity as the pH is increased [22]. The point of zero charge (ZPC) of Al(OH)₃ is known to be between pH 7.5 and 8.9 [23]. In the case of Al(OH)₃-coated NPs with ZPC at about pH

8–9, the adsorption capacity increased with increasing pH, mediated by the active hydroxyl group. Similarly, SiO₂ associated with ZPC of pH 2 offers improved adsorption capacity as pH increases [24].

DTZ (pK_a is 3.4) gets ionized at higher pH [20]. Uncoated iron oxide has better adsorption capacity

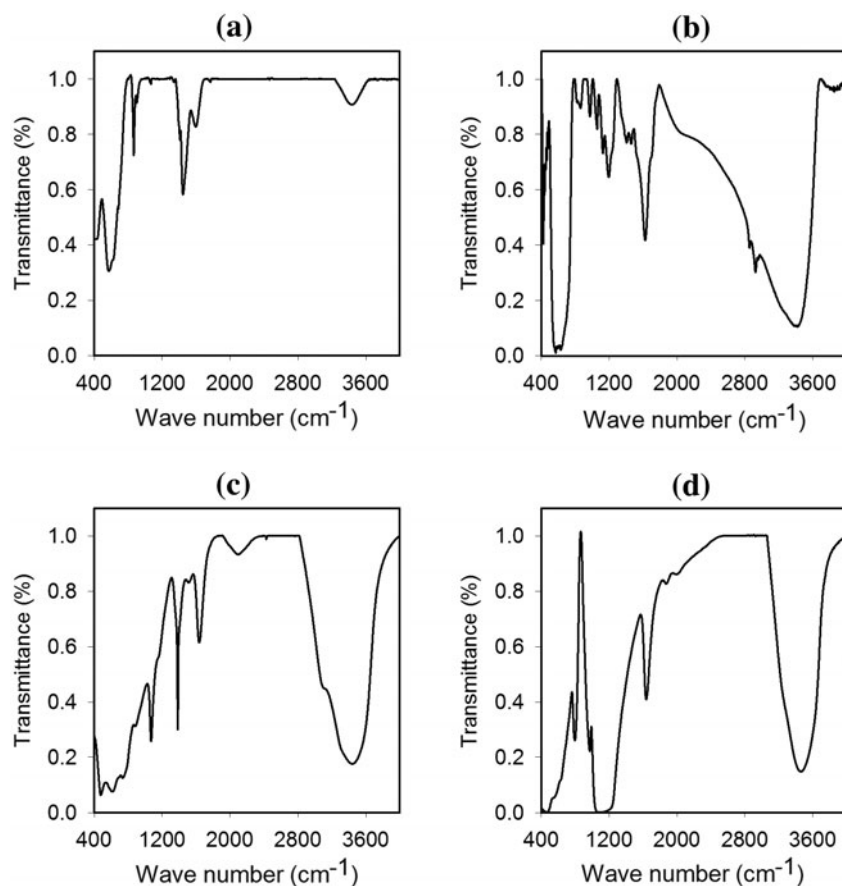


Fig. 4. The FT-IR results for (a) uncoated, (b) MAA-coated, (c) Al(OH)₃-coated, and (d) SiO₂-coated iron oxide nanoparticles (NPs).

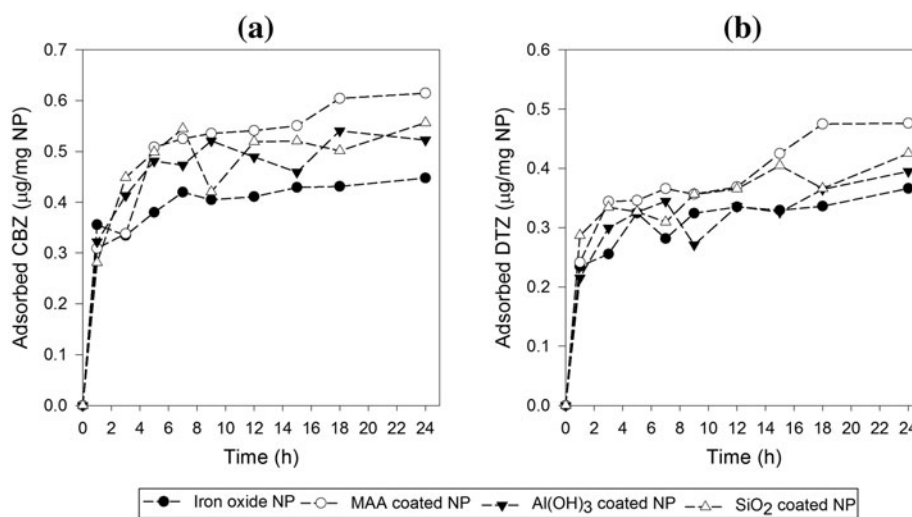


Fig. 5. Adsorption kinetics for each nanoparticles (NPs) toward (a) CBZ and (b) DTZ.

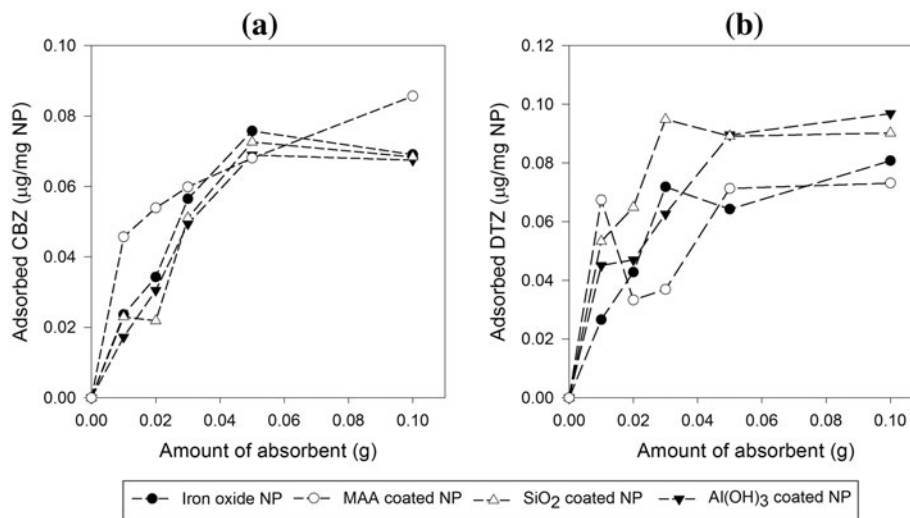


Fig. 6. Adsorption isotherm study with varying amount of surface-modified nanoparticles (NPs) as adsorbent for (a) CBZ and (b) DTZ.

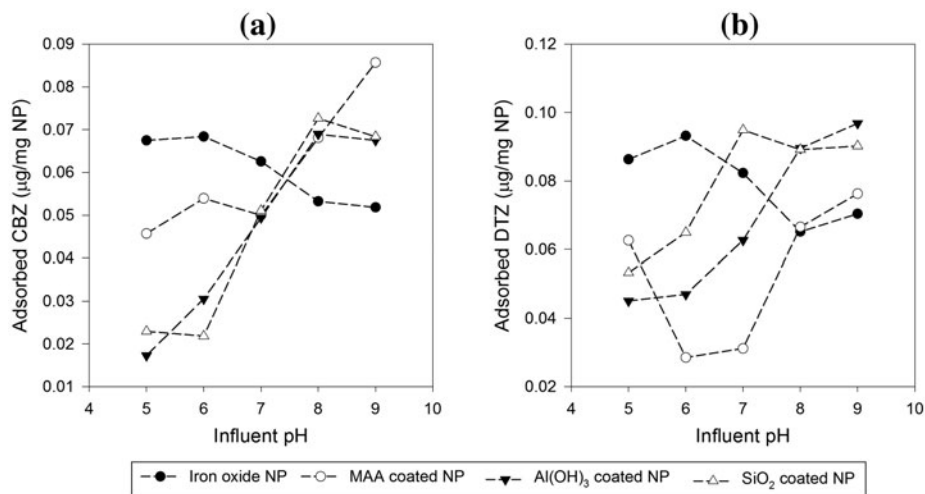


Fig. 7. Effect of influent pH on equilibrium adsorption capacity of different nanoparticles (NPs) toward (a) CBZ and (b) DTZ.

toward DTZ at lower pH (pH 5–6) than at higher pH (7–9). The NPs coated with Al(OH)_3 or SiO_2 showed better DTZ adsorption at pH 8–9, which is their effective ZPC range. Similarly, the adsorption capacity of MAA-coated NPs toward DTZ was most effective in the pH range of 8–9.

3.2.4. Effect of influent concentration on adsorption efficiency

The equilibrium adsorption isotherm model, i.e. drug adsorbed per gram of NP (q_e) vs. the equilibrium

concentration of drug in aqueous phase describes the interactive behavior between the two, and is important for predicting the adsorption capacity when designing an adsorption system. Equilibrium isotherm studies were carried out with different initial concentrations of CBZ/DTZ (0.1–100 mg/L) at 30°C and pH 8. The Freundlich [25] model was used to analyze the equilibrium adsorption data. Unlike Langmuir's model, the Freundlich isotherm describes the adsorption as multilayer on heterogeneous surface and interactions between adsorbed molecules [26]. The linearized form of the Freundlich adsorption isotherm equation is

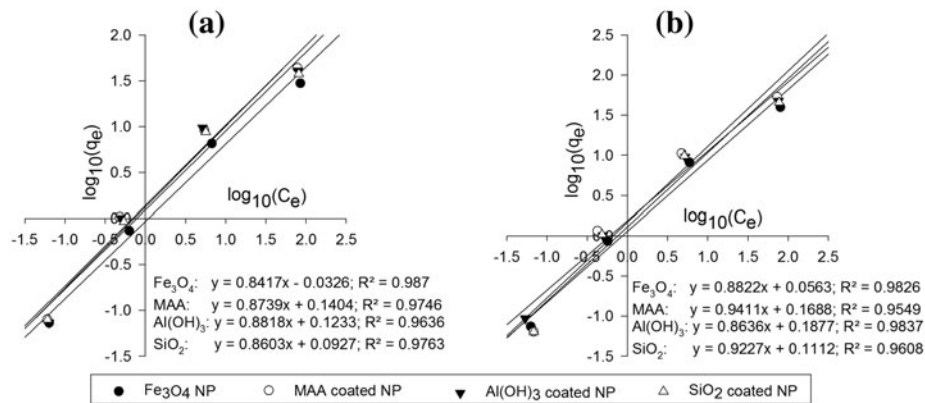


Fig. 8. Modeling experimental (a) CBZ and (b) DTZ adsorption by different nanoparticle (NPs) preparations to linearized Freundlich model. Best fit regression results are shown in incremental line types.

$$\ln q_e = \ln K_F + \left(\frac{1}{n}\right) \ln C_e \quad (1)$$

where C_e is the equilibrium concentration (mg/L) and q_e the amount of drug adsorbed at equilibrium (mg/g). K_F and n are Freundlich constants for the adsorbent–adsorbate pair, where n is related to the adsorption energy distribution and K_F indicates the adsorption capacity.

Equilibrium adsorption data were analyzed using the linearized form of the Freundlich equation, by plotting $\ln q_e$ vs. $\ln C_e$ as shown in Fig. 8. The calculated Freundlich isotherm constants and the corresponding correlation coefficient are shown in Table 2. Regression coefficients (R^2) for different conditions were larger than 0.95, indicating that the model fit reasonably well. In general, the adsorption capacity of an adsorbent increases with increasing K_F value. The estimated K_F

values from the DTZ adsorption isotherms suggested that the coated NPs had higher adsorption capacity than the original uncoated Fe₃O₄ NPs. The estimated maximum adsorption capacities of the MAA-coated NPs toward CBZ (77.30 mg/g) and DTZ (112.46 mg/g) were higher than those of the uncoated NPs (44.75 mg/g and 66.17 mg/g, respectively). The magnitude of the exponent “ n ” indicates the favorability of adsorption. The estimated n values of less than one with Al(OH)₃-coated and SiO₂-coated NPs toward CBZ suggested poor adsorption characteristics [27].

3.2.5. Optimal condition to remove CBZ and DTZ

The observations from previous batch adsorption test were considered while designing the optimal experimental conditions to maximize the adsorption of CBZ and DTZ. The optimal condition was chosen at individual concentrations of CBZ and DTZ at 100 μ g/L

Table 2

Parameters of the Freundlich isotherm for the adsorption of CBZ and DTZ onto nanoparticles (NPs)

Drug	Parameter	Nanoparticles (NPs)			
		Fe ₃ O ₄	Fe ₃ O ₄ –MAA	Fe ₃ O ₄ –Al(OH) ₃	Fe ₃ O ₄ –SiO ₂
CBZ	K_F	9.28	10.09	0.061	0.058
	n	1.19	1.02	0.92	0.88
	q_{\max}^a	44.75	77.30	77.07	65.05
	r^2	0.9870	0.9392	0.9636	0.9763
DTZ	K_F	10.43	11.69	14.29	10.73
	n	1.12	1.01	1.14	1.05
	q_{\max}^a	66.17	112.46	82.20	90.48
	r^2	0.9848	0.9723	0.9852	0.9719

^aThe theoretical maximum adsorption capacities (q_{\max}) have been deduced from regression of experimental data with Freundlich adsorption isotherm for an influent concentration (C_0) of 100 mg/L, where $\ln q_{\max}$ is the extrapolated value of $\ln q$ for $C_e = C_0$.

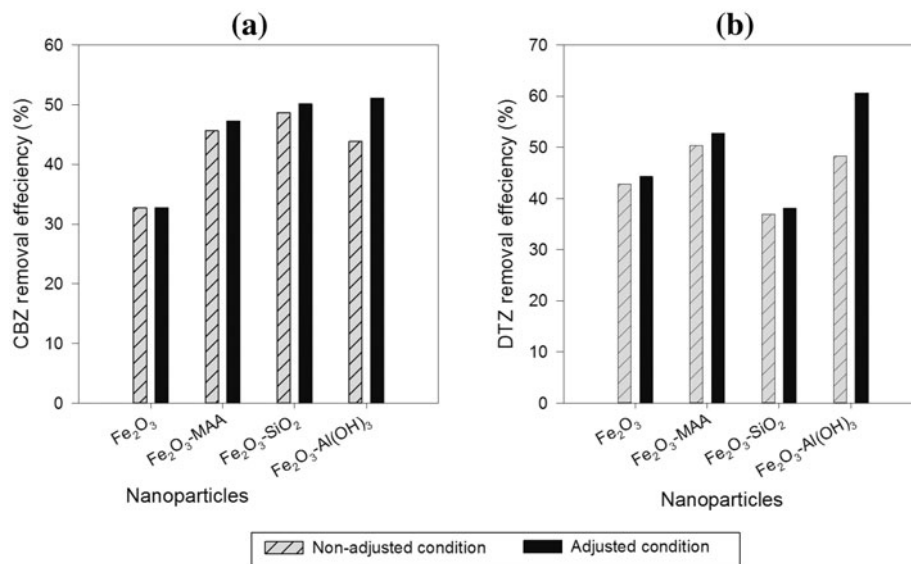


Fig. 9. Adsorptive removal for (a) CBZ and (b) DTZ by different nanoparticles (NPs) under adjusted (black solid bars) and nonadjusted (hatched bar) experimental conditions. The adjusted experimental condition was at pH 8 (except Fe₃O₄ where adjusted pH was 6) and incubation time of 7 h. Nonadjusted experiments received no pH regulation and incubation for 3 h.

with 0.05 g of NPs in 500 mL of influent at pH 8 and 7 h of incubation. The CBZ and DTZ removal under these selected optimized conditions and that of the earlier batch adsorption studies are shown in Fig. 9. The drug removal under optimal conditions differed among the various NPs. The optimal conditions did not necessarily improve the drug removal efficiency under the test conditions. Under the optimal experimental condition, CBZ removal with uncoated, MAA-coated, and SiO₂-

coated particles was improved by 0.05, 1.63, and 1.48%, respectively, in comparison to their respective removal efficiencies under the suboptimal condition. With the uncoated NPs, DTZ removal was 1.54% higher under the optimal condition than in the previous case. Similarly, DTZ removal with MAA-, SiO₂-, and Al(OH)₃-coated particles was improved by 2.39, 1.21, and 12.38%, respectively. The adsorption of CBZ and DTZ with Al(OH)₃-coated NPs at the selected pH and

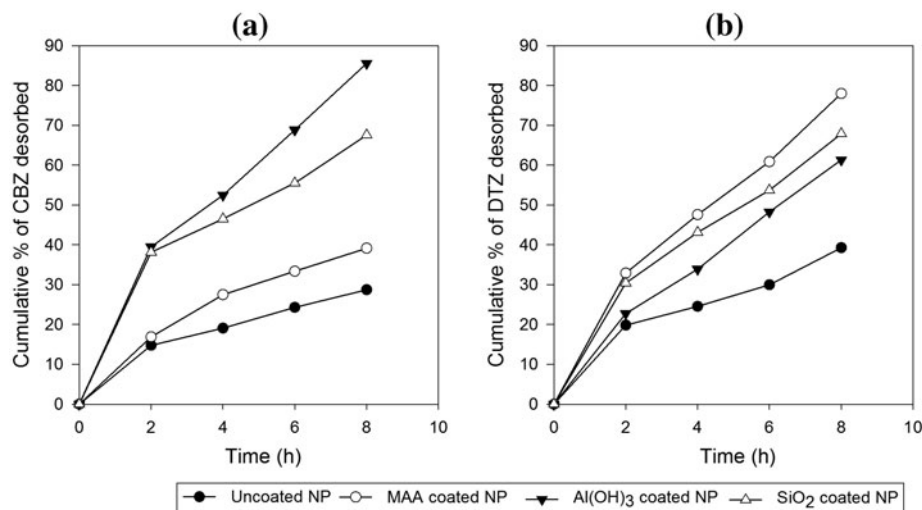


Fig. 10. Cumulative percentage release of (a) CBZ and (b) DTZ from coated and uncoated nanoparticles (NPs) in batch desorption test.

adsorption time was greatly improved when compared to the uncoated one. We anticipate that the adsorption kinetics with $\text{Al}(\text{OH})_3$ would have been very slow, and the equilibrium time envisaged in earlier studies might not be appropriate, because the adsorption was presumed to have continued even after equilibrium.

3.3. Desorption of CBZ and DTZ from uncoated and coated iron oxide NPs

The desorption profiles of CBZ and DTZ from preadsorbed NPs are shown in Fig. 10. From the uncoated NPs, only 28.72 and 39.25% of CBZ and DTZ was desorbed, respectively. However, about 85.56% of CBZ and 78.00% of DTZ could be desorbed from $\text{Al}(\text{OH})_3$ - and MAA-coated NPs, respectively. Significantly, this high desorption was achieved within about 8 h, which is a similar period to their adsorption equilibrium. This was possibly attributed to the absence of internal diffusion resistance in those drug-NP combinations.

4. Conclusion

This study suggests that surface-modified NPs (with organic/inorganic modifier) may be a valuable tool in the removal of very low concentrations of persistent drugs such as CBZ and DTZ. The adsorption capacity of the surface-modified NPs was superior to that of the original NPs. With further adjustment of drug and/or NP concentration, reaction time, and solution pH, the adsorption capacity can be further improved. The high level of drug desorption attained using the coated NPs, in a time frame equivalent to the adsorption equilibrium, supports their potential application in water and wastewater treatment.

Acknowledgment

This work was supported by a grant from “Kor-Indo Savi program” by the National Research Foundation of Korea (NRF) (NRF-2013K2A1B9065411) and “The GAIA Project” funded by the Korea Ministry of Environment (2014000550004).

References

- [1] Y. Zhang, S. Geissen, C. Gal, Carbamazepine and diclofenac: Removal in wastewater treatment plants and occurrence in water bodies, *Chemosphere* 73 (2008) 1151–1161.
- [2] T.A. Ternes, Occurrence of drugs in German sewage treatment plants and rivers1 dedicated to Professor Dr. Klaus Haberer on the occasion of his 70th birthday.1, *Water Res.* 32 (1998) 3245–3260.
- [3] U.S. EPA, 2012, Available from: <<http://water.epa.gov/scitech/cec/>>.
- [4] A. Haiss, K. Kümmerer, Biodegradability of the X-ray contrast compound diatrizoic acid, identification of aerobic degradation products and effects against sewage sludge micro-organisms, *Chemosphere* 62 (2006) 294–302.
- [5] S. Pérez, D. Barceló, Fate and occurrence of X-ray contrast media in the environment, *Anal. Bioanal. Chem.* 387 (2007) 1235–1246.
- [6] M.E. McHenry, D.E. Laughlin, Nano-scale materials development for future magnetic applications, *Acta Mater.* 48 (2000) 223–238.
- [7] B. Pan, H. Qiu, B. Pan, G. Nie, L. Xiao, L. Lv, W. Zhang, Q. Zhang, S. Zheng, Highly efficient removal of heavy metals by polymer-supported nanosized hydrated Fe(III) oxides: Behavior and XPS study, *Water Res.* 44 (2010) 815–824.
- [8] R.D. Ambashta, M. Sillanpää, Water purification using magnetic assistance: A review, *J. Hazard. Mater.* 180 (2010) 38–49.
- [9] J. Hu, G. Chen, I.M.C. Lo, Removal and recovery of Cr (VI) from wastewater by maghemite nanoparticles, *Water Res.* 39 (2005) 4528–4536.
- [10] X. Li, W. Zhang, Iron nanoparticles: the core-shell structure and unique properties for Ni(II) sequestration, *Langmuir* 22 (2006) 4638–4642.
- [11] U. Jeong, X. Teng, Y. Wang, H. Yang, Y. Xia, Superparamagnetic colloids: Controlled synthesis and niche applications, *Adv. Mater.* 19 (2007) 33–60.
- [12] L. Machala, R. Zboril, A. Gedanken, Amorphous iron (III) oxide a review, *J. Phys. Chem. B* 111 (2007) 4003–4018.
- [13] Y. Lu, Y. Yin, B.T. Mayers, Y. Xia, Modifying the surface properties of superparamagnetic iron oxide nanoparticles through a sol-gel approach, *Nano Lett.* 2 (2002) 183–186.
- [14] S. Yu, G.M. Chow, Carboxyl group ($-\text{CO}_2\text{H}$) functionalized ferrimagnetic iron oxide nanoparticles for potential bio-applications, *J. Mater. Chem.* 14 (2004) 2781–2786.
- [15] X. Zhao, J. Wang, F. Wu, T. Wang, Y. Cai, Y. Shi, G. Jiang, Removal of fluoride from aqueous media by $\text{Fe}_3\text{O}_4@ \text{Al}(\text{OH})_3$ magnetic nanoparticles, *J. Hazard. Mater.* 173 (2010) 102–109.
- [16] H. Hu, Z. Wang, L. Pan, Synthesis of monodisperse $\text{Fe}_3\text{O}_4@ \text{silica}$ core-shell microspheres and their application for removal of heavy metal ions from water, *J. Alloys Compd.* 492 (2010) 656–661.
- [17] P. Tartaj, M. Morales, S. Veintemillas-Verdaguer, T. González-Carretero, C. Serna, The preparation of magnetic nanoparticles for applications in biomedicine, *J. Phys. D: Appl. Phys.* 36 (2003) R182–R197.
- [18] S. Yean, L. Cong, C.T. Yavuz, J.T. Mayo, W.W. Yu, A.T. Kan, V.L. Colvin, M.B. Tomson, Effect of magnetite particle size on adsorption and desorption of arsenite and arsenate, *J. Mater. Res.* 20 (2005) 3255–3264.
- [19] H.A. Al-Abadleh, V.H. Grassian, FT-IR study of water adsorption on aluminum oxide surfaces, *Langmuir* 19 (2003) 341–347.

- [20] D.Barceló, M.Petrovic, *Emerging Contaminants from Industrial and Municipal Waste*, Springer, 2008, pp. 103–126, ISBN 978-3-540-79209-3, doi: [10.1007/978-3540-79210-9](https://doi.org/10.1007/978-3540-79210-9).
- [21] S. Santra, R. Tapeç, N. Theodoropoulou, J. Dobson, A. Hebard, W. Tan, Synthesis and characterization of silica-coated iron oxide nanoparticles in microemulsion: The effect of nonionic surfactants, *Langmuir* 17 (2001) 2900–2906.
- [22] C.C. Berry, A.S.G. Curtis, Functionalisation of magnetic nanoparticles for applications in biomedicine, *J. Phys. D: Appl. Phys.* 36 (2003) R198–R206.
- [23] J. Rosenqvist, P. Persson, S. Sjöberg, Protonation and charging of nanosized gibbsite (α -Al(OH)₃) particles in aqueous suspension, *Langmuir* 18 (2002) 4598–4604.
- [24] Y.G. Jung, U. Paik, Fabrication of *in-situ* formed nanocomposite using polymer precursor: I. Adsorption behavior of polymer followed SiO₂ surface formation onto silicon nitride surface, *J. Korean Ceram. Soc.* 37 (2000) 280–287.
- [25] H. Freundlich, W. Heller, The Adsorption of cis- and trans-azobenzene, *J. Am. Chem. Soc.* 61 (1939) 2228–2230.
- [26] S. Chatterjee, D.S. Lee, M.W. Lee, S.H. Woo, Enhanced adsorption of congo red from aqueous solutions by chitosan hydrogel beads impregnated with cetyl trimethyl ammonium bromide, *Bioresour. Technol.* 100 (2009) 2803–2809.
- [27] O. Hamdaoui, E. Naffrechoux, Modeling of adsorption isotherms of phenol and chlorophenols onto granular activated carbon: Part I. Two-parameter models and equations allowing determination of thermodynamic parameters, *J. Hazard. Mater.* 147 (2007) 381–394.